Delft University of Technology

Online Lithium-ion Battery Modeling and State of Charge Estimation via Concurrent State and Parameter Estimation

Li, Jimei; Wang, Yang; Ferrari, Riccardo M.G.; Swevers, Jan; Ding, Feng

Important note
To cite this publication, please use the final published version (if applicable).
Please check the document version above.

Online Lithium-ion Battery Modeling and State of Charge Estimation via Concurrent State and Parameter Estimation[★]

Jimei Li [*,**] **Yang Wang** [***] **Riccardo M.G. Ferrari** [***]
Jan Swevers [**] **Feng Ding** [*]

[*] *School of Internet of Things Engineering, Jiangnan University, Wuxi
214122, PR China (e-mail: jimeili0625@163.com,
fding@jiangnan.edu.cn)*
[**] *MECO Research Team, Dept. Mechanical Engineering, KU Leuven.
Flanders Make@KU Leuven, 3001 leuven, Belgium (e-mail:
jan.swevers@kuleuven.be)*
[***] *Delft Center for Systems and Control, Delft University of
Technology, Mekelweg 2, 2628 CD, Delft, The Netherlands (e-mail:
y.wang-40, r.ferrari@tudelft.nl)*

Abstract: This paper develops a novel approach for online Lithium-ion (Li-ion) battery model identification and state of charge (SOC) estimation. To account for the SOC-dependent battery dynamics and the static nonlinearity between the open-circuit voltage (OCV) and SOC, we formulate a grey box nonlinear state-space model, in which elements depend on SOC in a polynomial way. For model identification, we propose an online concurrent state and parameter estimation by alternating the recursive least squares algorithm and particle filter; the SOC is computed via Coulomb counting during the modeling. The identified grey box model is then applied for SOC estimation using the particle filter. Simulation with real-world battery measurements demonstrates the effectiveness of the model structure and the estimation approach, which is reflected in accurate terminal voltage estimation and nonlinear OCV-SOC relation, and superior performance regarding SOC estimation compared to state-of-the-art approaches.

Keywords: Li-ion battery modeling; equivalent circuit model; nonlinear system identification; SOC estimation; least squares; particle filter.

1. INTRODUCTION

Lithium-ion (Li-ion) batteries, known for their high energy density and extended service life, are the most promising energy storage systems for electric vehicles (EVs) (Meng et al. (2018), Plett (2015)). The state of charge (SOC) of batteries, indicating the amount of charge in the cell is a crucial battery state for the safety and functionality of EV applications. Accurate estimation of SOC prevents the battery from over-charging and over-discharging and thus ensures reliable EV operation. Equivalent circuit models (ECMs) are favorable models for EVs to describe battery behaviors due to their decent balance between accuracy and computational cost (Tian et al. (2023)). The accuracy of the SOC depends on the fidelity of the battery model (Shrivastava et al. (2019)).

Battery dynamics are governed by complex electrochemical processes hidden in battery cells and exhibit a complex nonlinear input-output dynamic changing with the SOC value. To accommodate this, ECM parameters, which determine the dynamic voltage of the battery, exhibit a nonlinear and time-varying dependency on the SOC. Additionally, the open-circuit voltage (OCV), which decides the steady-state voltage of the cell, is a static nonlinear SOC function. The dynamic voltage and the OCV form the terminal voltage of the battery cell, and cannot be measured separately, thereby increasing the complexity of ECM identification.

The conventional approach (Tran et al. (2021)) to estimate the parameters of nonlinear ECMs, is to conduct dedicated battery tests that allow for direct measurement of individual model parameters. However, these test-based approaches are time- and labor-intensive because they require repetition for various working conditions under laboratory environments, making them impractical for real-world applications. Online estimation algorithms such as the extended Kalman filter (Plett (2004)) and the recursive least squares estimation (Wang et al. (2023)) have been applied to track the time evolution of the ECM parameters using instantaneous data measurement. However, these approaches regard the ECMs as time-varying models and do not account for the state-dependent characteristics of the ECM parameters. Desai et al. (2023) developed a

SOC-dependent ECM with a moving horizon estimator for joint state and parameter estimation. Nonetheless, this approach requires a specially designed hybrid pulse power characterization (HPPC) test signal for the intended estimation and hence is not directly applicable to normal battery operations.

Contributions: In this work, we develop a time-invariant model structure, which explicitly includes the dependency of the model parameters on the SOC through polynomials. This formulation offers higher fidelity for capturing the nonlinear battery dynamics. For the developed nonlinear state-space battery model, we propose an online concurrent state and parameter estimation method for identifying the model parameters and reconstructing the nonlinear OCV-SOC curve. This approach alternates between the recursive least squares algorithm and the particle filter to resolve the interdependency between states and parameters involved in the model structure. With the identified battery model, we realize online SOC estimation using the particle filter. The proposed model structure and the estimation method are tested using NMC/Graphite Li-ion battery dynamic driving test datasets. The contributions of this paper are summarized as follows:

- The conventional time-varying ECM is reformulated as a time-invariant nonlinear grey box state-space model;
- A particle filter-recursive least squares (PF-RLS) algorithm is proposed to estimate the grey box state-space model and the nonlinear OCV-SOC curve;
- Based on the identified model, the online SOC estimation is realized using the particle filter;
- Simulation experiments are conducted to validate the developed approach, showing an enhanced performance in model output fitting and SOC estimation compared to the state-of-the-art methods.

The rest of the paper is structured as follows. Section 2 develops a grey box nonlinear state-space model for Li-ion batteries. Section 3 proposes an online concurrent state and parameter estimation method for the developed model. Section 4 validates the proposed modeling framework on NMC/Graphite Li-ion battery identification experiments. Finally, some concluding remarks are given in Section 5.

2. MODEL DEVELOPMENT

The equivalent circuit model (ECM) we consider in this work is the second-order Thevinin's model as shown in Fig. 1. This model consists of an ideal voltage source v_{ocv}, an ohmic resistance R_0, and two resistor-capacitor (RC) networks, $R_i, C_i, i = 1, 2$. i_b is the load current (positive for charging), v_b is the terminal voltage, v_0, v_1, and v_2 are the voltage drops across R_0 and the two RC networks respectively, and v_{ocv} is the open-circuit voltage (OCV).

According to Kirchhoff's law, the dynamics of the ECM are described by the following differential equations:

$$\dot{v}_{1,t} = -\frac{1}{\tau_1(p_t)}v_{1,t} + \frac{1}{C_1(p_t)}i_{b,t}, \tag{1}$$

$$\dot{v}_{2,t} = -\frac{1}{\tau_2(p_t)}v_{2,t} + \frac{1}{C_2(p_t)}i_{b,t}, \tag{2}$$
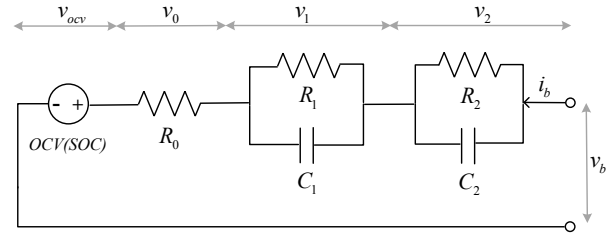

Fig. 1. Second-order Thevinin's equivalent circuit.

where $p_t \in [0, 1]$ is the state of charge (SOC), $\tau_1 := R_1 C_1$ and $\tau_2 := R_2 C_2$ are the time constants of the $v_{1,t}$, $v_{2,t}$ dynamics respectively. The ECM terminal voltage is

$$v_{b,t} = v_{1,t} + v_{2,t} + R_0(p_t)i_{b,t} + v_{ocv}(p_t).$$

The ECM parameters, $R_i, C_j, i = 0, 1, 2, j = 1, 2$, and the OCV vary with the SOC which describes the amount of charge in a cell relative to its total capacity (Chen and Rincon-Mora (2006)). The SOC has a dynamic as follows:

$$\dot{p}_t = \frac{\eta}{C_p}i_{b,t}, \tag{3}$$

where $\eta \in [0, 1]$ is the coulombic efficiency and $C_p \in \mathbb{R}^+$ is the total capacity of the battery defined in Coulombs (C).

Discretizing Equations (1)–(3) by finite difference approximation $\dot{x}_k = (x_{k+1} - x_k)/T_s$, we can write a discrete-time state-space model of the ECM as

$$\begin{bmatrix} v_{1,k+1} \\ v_{2,k+1} \\ p_{k+1} \end{bmatrix} = \begin{bmatrix} 1 - \dfrac{T_s}{\tau_1(p_k)} & 0 & 0 \\ 0 & 1 - \dfrac{T_s}{\tau_2(p_k)} & 0 \\ 0 & 0 & 1 \end{bmatrix} \times \begin{bmatrix} v_{1,k} \\ v_{2,k} \\ p_k \end{bmatrix} +$$
$$\begin{bmatrix} \dfrac{T_s}{C_1(p_k)} & \dfrac{T_s}{C_2(p_k)} & \dfrac{T_s\eta}{C_p} \end{bmatrix}^\top i_{b,k}, \tag{4}$$

$$v_{b,k} = v_{1,k} + v_{2,k} + R_0(p_k)i_{b,k} + v_{ocv}(p_k), \tag{5}$$

where $T_s = 1$s is the sampling time for the discretization.

According to studies (Chen and Rincon-Mora (2006), Tian et al. (2020)), state-space parameters in (4)–(5) are approximately a linear function of the SOC, and the OCV-SOC nonlinearity presents proximity to a fourth-order polynomial. With this consideration, we derive the following time-invariant grey box nonlinear state-space model,

$$\begin{bmatrix} v_{1,k+1} \\ v_{2,k+1} \\ p_{k+1} \end{bmatrix} = \begin{bmatrix} \alpha_0 + \alpha_1 p_k & 0 & 0 \\ 0 & \beta_0 + \beta_1 p_k & 0 \\ 0 & 0 & 1 \end{bmatrix} \times \begin{bmatrix} v_{1,k} \\ v_{2,k} \\ p_k \end{bmatrix} +$$
$$\begin{bmatrix} \mu_0 + \mu_1 p_k & \zeta_0 + \zeta_1 p_k & \dfrac{T_s\eta}{C_p} \end{bmatrix}^\top i_{b,k}, \tag{6}$$

$$v_{b,k} = v_{1,k} + v_{2,k} + [\gamma_0 + \gamma_1 p_k]i_{b,k} +$$
$$\theta_0 + \theta_1 p_k + \theta_2 p_k^2 + \theta_3 p_k^3 + \theta_4 p_k^4. \tag{7}$$

This formulation incorporates the inherent SOC-dependent dynamics directly into the model structure and thus allows for more accurate capturing of battery dynamics.

For identifying the nonlinear state-space model (6)–(7), we assume that the coulombic efficiency η and the battery capacity C_p are known. It is also commonly assumed in literature (Fan et al. (2022), Zhang et al. (2018)). This assumption allows us to compute a reference SOC using (3) and construct a SOC-dependent battery model associated

with the reference value. For the remaining of this paper, we assume that $\eta = 1$ and $C_p = 7200C$. In addition, we assume that the ambient temperature is constant and the charging-discharging rate is small enough, such that no significant heat is generated inside the battery.

Directly applying (3) for online battery SOC estimation is an open-loop approach that will suffer from accumulated measurement errors and inaccuracy of the initial SOC. An accurate battery model is thus required to achieve a closed-loop estimation that can correct the SOC when it is contaminated by large errors.

With the above model formulation and assumptions, this work aims to estimate the polynomial coefficients of the nonlinear model (6)–(7) based on the input-output measurements and to estimate the SOC online with the identified battery model.

3. METHODOLOGY

The estimation of polynomial coefficients of the nonlinear state-space model (6)–(7) is based on alternately identifying the coefficients and the unmeasurable system states. A recursive least squares method is first applied to estimate the model parameters, and then a particle filter (PF) is used to estimate the current state variable using the updated system model. This procedure is performed iteratively throughout the entire data length L.

3.1 Parameter estimation with RLS algorithm

According to the nonlinear state-space model (6)–(7), we substitute the state update equation into the output equation, yielding the following regression form:

$$
\begin{aligned}
v_{b,k} = &(\alpha_0 + \alpha_1 p_{k-1})v_{1,k-1} + (\mu_0 + \mu_1 p_{k-1})i_{b,k-1} \\
&+ (\beta_0 + \beta_1 p_{k-1})v_{2,k-1} + (\zeta_0 + \zeta_1 p_{k-1})i_{b,k-1} \\
&+ (\gamma_0 + \gamma_1 p_k)i_{b,k} + \theta_0 + \theta_1 p_k + \theta_2 p_k^2 + \theta_3 p_k^3 + \theta_4 p_k^4.
\end{aligned} \tag{8}
$$

The polynomial coefficients involved in (8) can be estimated by solving the following problem,

$$
\min_{\boldsymbol{\vartheta}} \sum_{j=1}^{k} [v_{b,j} - \boldsymbol{\psi}_j^\top \boldsymbol{\vartheta}]^2, \tag{9}
$$

where $\boldsymbol{\psi}_k \in \mathbb{R}^{15}$ is the information vector containing all combinations of the state variables presented in (8), and $\boldsymbol{\vartheta} \in \mathbb{R}^{15}$ is the vector of the corresponding polynomial coefficients to be estimated. Let $\hat{\boldsymbol{\vartheta}}_k$ be the estimate of $\boldsymbol{\vartheta}$ at the sampling instant k, we apply the RLS algorithm to recursively update $\hat{\boldsymbol{\vartheta}}_k$ by the following relation,

$$
\hat{\boldsymbol{\vartheta}}_k = \hat{\boldsymbol{\vartheta}}_{k-1} + \boldsymbol{L}_k[v_{b,k} - \boldsymbol{\psi}_k^\top \hat{\boldsymbol{\vartheta}}_{k-1}], \tag{10}
$$

$$
\boldsymbol{L}_k = \boldsymbol{P}_{k-1}\boldsymbol{\psi}_k[1 + \boldsymbol{\psi}_k^\top \boldsymbol{P}_{k-1}\boldsymbol{\psi}_k]^{-1}, \tag{11}
$$

$$
\boldsymbol{P}_k = [\boldsymbol{I}_{15} - \boldsymbol{L}_k\boldsymbol{\psi}_k^\top]\boldsymbol{P}_{k-1}, \tag{12}
$$

where $\boldsymbol{L}_k \in \mathbb{R}^{15}$ is the gain vector and $\boldsymbol{P}_k \in \mathbb{R}^{15 \times 15}$ is the covariance matrix. The state p_k is computed using the current integration (3), and the unknown voltages v_1 and v_2 in $\boldsymbol{\psi}_k$ are estimated by the PF algorithm introduced in the next subsection.

3.2 State estimation with PF algorithm

The particle filter is an attractive approach to estimate the states of nonlinear state-space models. With the system model updated by the RLS method, we apply the PF to estimate the state variables v_1 and v_2 according to the output measurements so that the alternate PF-RLS algorithm converges to the true state and parameter pairs.

In PFs, the posterior density function of system states is represented by a set of random particles $\{\hat{\boldsymbol{x}}_k^n\}_{n=1}^N$ and associated weights $\{w_k^n\}_{n=1}^N$:

$$
p(\boldsymbol{x}_k|\boldsymbol{V}_{1:k}, \boldsymbol{I}_{1:k}, \hat{\boldsymbol{\vartheta}}_{1:k}) \approx \sum_{n=1}^{N} w_k^n \delta(\boldsymbol{x}_k - \hat{\boldsymbol{x}}_k^n), \tag{13}
$$

where $\boldsymbol{x}_k = [v_{1,k}, v_{2,k}]^\top \in \mathbb{R}^2$ is the state vector, $\boldsymbol{V}_{1:k} := \{v_{b,1}, v_{b,2}, \cdots, v_{b,k}\}$ and $\boldsymbol{I}_{1:k} := \{i_{b,1}, i_{b,2}, \cdots, i_{b,k}\}$ are the sequences of the input-output measurements, and $\hat{\boldsymbol{\vartheta}}_{1:k} := \{\hat{\boldsymbol{\vartheta}}_1, \hat{\boldsymbol{\vartheta}}_2, \cdots, \hat{\boldsymbol{\vartheta}}_k\}$ is a sequence containing the estimated parameter vectors. $\delta(\cdot)$ denotes the Dirac delta function, and N is the number of particles.

Using the sequential importance sampling, the weights in Equation (13) are updated recursively by the likelihood of having output $v_{b,k}$ given particle $\hat{\boldsymbol{x}}_k^n$, input $i_{b,k}$ and parameter vector $\hat{\boldsymbol{\vartheta}}_k$:

$$
w_k^n = w_{k-1}^n p(v_{b,k}|\hat{\boldsymbol{x}}_k^n, i_{b,k}, \hat{\boldsymbol{\vartheta}}_k), \tag{14}
$$

where $p(v_{b,k}|\hat{\boldsymbol{x}}_k^n, i_{b,k}, \hat{\boldsymbol{\vartheta}}_k)$ is a probability density function. The details on sequential importance sampling can be found in (Arulampalam et al. (2002)). The probability density function in (14) is commonly selected as the Gaussian distribution,

$$
p(v_{b,k}|\hat{\boldsymbol{x}}_k^n, i_{b,k}, \hat{\boldsymbol{\vartheta}}_k) = \frac{1}{\sqrt{2\pi}\sigma_v} \exp\left\{ -\frac{[v_{b,k} - \hat{v}_{b,k}^n]^2}{2\sigma_v^2} \right\},
$$

where $\hat{v}_{b,k}^n$ is the predicted output from the particle $\hat{\boldsymbol{x}}_k^n$, and σ_v^2 is the variance of the measurement noise. After each weight update, we normalize w_k^n with

$$
\bar{w}_k^n = w_k^n / \sum_{n=1}^{N} w_k^n, \tag{15}
$$

so that the normalized weights satisfy $\sum_{n=1}^{N} \bar{w}_k^n = 1$.

The degeneracy phenomenon is an inevitable problem in particle filters, which causes the computational effort spent on particles with small weights that degenerate the PF performance. Degeneracy is typically monitored using the efficient sampling number N_{eff} defined as:

$$
N_{\text{eff}} := \left[\sum_{n=1}^{N} (\bar{w}_k^n)^2 \right]^{-1}. \tag{16}
$$

A small N_{eff} indicates a degraded performance of the PF method, as it has only a few useful large-weight particles. Thus, If N_{eff} decreases below a prior set threshold N_{hold}, we apply the so-called **systematic resampling** (Li et al. (2015)) with high computational efficiency to recover the degeneracy phenomenon.

To this aim, we calculate the cumulative sum of the normalized weights $W_k^n = \sum_{i=1}^{n} \bar{w}_k^i$ for particles up to the n-th one, and draw a random number h_k^1 from the

uniform distribution on $(0, \frac{1}{N}]$; the remaining elements are obtained by $h_k^n = h_k^1 + (n-1)/N$, for $n = 2, 3, \cdots, N$. During resampling, we duplicate the n-th particle $\boldsymbol{x}_k^n$ to the j-th one when the element of the j-th one satisfies the following condition:

$$W_k^{n-1} < h_k^j < W_k^n. \tag{17}$$

By this procedure, we keep large-weight particles exploiting the fact that the larger the normalized weight is, the higher the probability of h_k^j falls between the boundaries indicated in (17). Finally, we reset the weight $\bar{w}_k^n$ of each particle as $1/N$.

The state estimates can then be updated by a series of weighted samples as,

$$\hat{\boldsymbol{x}}_k = \sum_{n=1}^{N} \bar{w}_k^n \hat{\boldsymbol{x}}_k^n. \tag{18}$$

With the estimated states, the RLS algorithm is applied to estimate the polynomial coefficients of the nonlinear state-space model in the next iteration, achieving concurrent state and parameter estimation. The procedures of the developed particle filter-recursive least squares (PF-RLS) algorithm are given in **Algorithm 1**.

Algorithm 1 PF-RLS algorithm

Initialization: : $\hat{\boldsymbol{\vartheta}}_0, \{\hat{\boldsymbol{x}}_{k-i}\}_{i=1}^2, \{\hat{\boldsymbol{x}}_0^n\}_{n=1}^N, \{w_0^n\}_{n=1}^N$.
1: **for** $k = 1 : L$ **do**
2:      Form the information vector $\hat{\boldsymbol{\psi}}_k$.   ▷ RLS
3:      Compute the gain vector $\boldsymbol{L}_k$ by (11).
4:      Calculate the matrix $\boldsymbol{P}_k$ by (12).
5:      Update the parameter vector $\hat{\boldsymbol{\vartheta}}_k$ by (10).
6:      **for** $n = 1 : N$ **do**   ▷ PF
7:          Propagate particles through (6).
8:          Compute the output of each particle by (7).
9:          Assign the weight of each particle by (14).
10:      **end for**
11:      Normalize weights by (15).
12:      Compute N_{eff} by (16).
13:      **if** $N_{\text{eff}} < N_{\text{hold}}$ **then**
14:          Perform systematic resampling.
15:      **end if**
16:      Reset the weight of each particle to $\frac{1}{N}$.
17:      Update the state estimates $\hat{\boldsymbol{x}}_k$ according to (18).
18: **end for**

3.3 Online SOC estimation with PF algorithm

Based on the estimated nonlinear state-space model (6)–(7) and the measurements $\{i_{b,k}, v_{b,k}, k = 1, 2, \cdots, L\}$ from validation datasets, we apply the PF algorithm from Line 6 to 15 in **Algorithm 1** to estimate the SOC of the battery. Here, the state vector is defined as $\boldsymbol{x}_k = [v_{1,k}, v_{2,k}, p_k]^\top \in \mathbb{R}^3$. The closed-loop estimation ensures a correction of the SOC towards the reference value computed during the modeling stage when the current estimate is contaminated with large errors.

4. EXPERIMENTS AND RESULTS

In this section, we evaluate the performance of the PF-RLS algorithm for online battery modeling and SOC estima-

tion. The dataset we adopt in the simulation experiments is from the CALCE dataset (Zheng et al. (2016)).

Fig. 2 shows the procedure of the simulation experiments. We first perform the concurrent state and parameter estimation for constructing a nonlinear state-space model (6)–(7) using measurements under dynamic driving conditions. Then with the estimated model, we use the particle filter for SOC estimation. The nonlinear battery model is constructed with the Dynamic Stress Test (DST) profile and the SOC estimation is evaluated on the more sophisticated Federal Urban Driving Schedule (FUDS) and the Beijing Dynamic Stress Test (BJDST) profiles. All test data are collected from LiNiMnCo(NMC)/Graphite batteries with 80% initial SOC under constant temperature conditions.
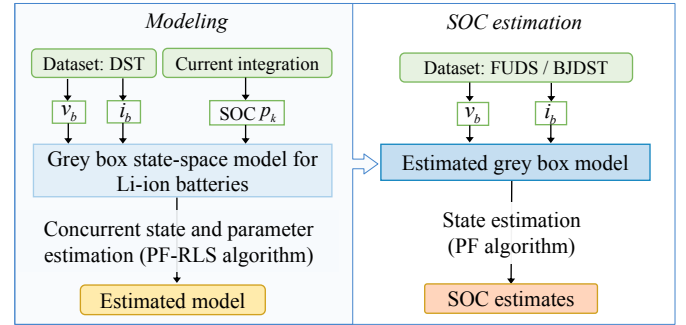

Fig. 2. The procedure of experiments.

For modeling, we evaluate the accuracy of the terminal voltage fitting and the OCV-SOC curve reconstruction. In the SOC estimation, we assess the effectiveness of the developed method to follow the reference SOC and recover the estimate from inaccurate initial values. The root mean squares error (RMSE) is calculated to evaluate the estimation precision of the proposed algorithm.

4.1 Modeling

In the modeling experiment, we estimate polynomial coefficients of the nonlinear state-space model (6)–(7) using the DST dataset collected at 0 °C, 25 °C, and 45 °C. The performance of the proposed PF-RLS method is evaluated by the fitting accuracy of the estimated terminal voltage to measurements.

The SOC is computed by concurrent integration using (3) with initial value $p_0 = 0.8$. For the RLS algorithm, the initial covariance matrix is taken as $\boldsymbol{P}_0 = \boldsymbol{I}_{15}$. In the PF, the initial state is taken as $\boldsymbol{x}_0 = \boldsymbol{1}_2/10^6$. N initial particles are drawn from a Gaussian distribution function $\mathcal{N}(\boldsymbol{x}_0, \sigma_x^2)$ with mean $\boldsymbol{x}_0$ and variance $\sigma_x^2 = 3$ [V^2]. The number of particles N is set as 1000. The initial weights satisfy $\{w_0^n\}_{n=1}^N = 1/N$. The variances of the process noise σ_w^2 and measurement noise σ_v^2 are set as $\sigma_w^2 = 10^{-4}$ [V^2] and $\sigma_v^2 = 10^{-8}$ [A^2] according to the statistic analysis. The threshold value for resampling is taken as $N_{\text{hold}} = N$, yielding that the resampling is performed at each iteration.

Fig. 3 shows the comparison of terminal voltage estimates with the measurements and the estimation errors on the DST dataset at 0 °C, 25 °C and 45 °C. The PF-RLS algorithm accurately tracks the actual terminal voltage in time even when the actual voltage changes drastically. Table 1

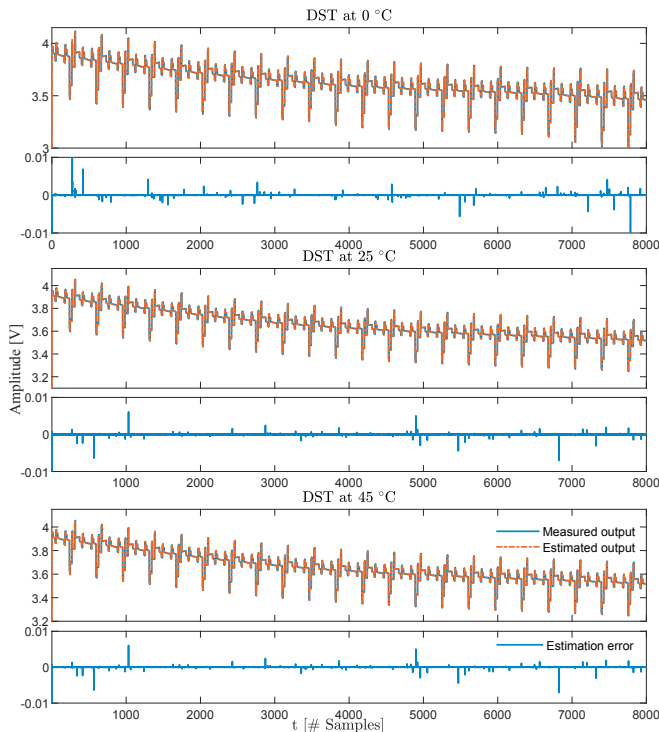shows the RMSE [mV] in terminal voltage estimated by the PF-RLS algorithm.

Fig. 3. Terminal voltage estimation results under DST at three different constant temperatures.

Table 1. RMSE [mV] of terminal voltage estimates under DST at different temperatures.

Approach	0 °C	25 °C	45 °C
PF-RLS	1.40	0.19	0.21

As shown in Fig. 3 and Table 1, the PF-RLS algorithm has a high estimation accuracy and the low RMSE on the terminal voltage estimation at three temperatures. The developed nonlinear state-space model with concurrent estimation method has a satisfactory performance in describing the battery input-output behaviors.

For further validation, we compare the estimated OCV-SOC curves with the averaged OCV-SOC curves obtained from the incremental current OCV test collected in the CALCE dataset. Fig. 4 shows the OCV-SOC curve comparison under DST at different temperatures, from which we can see that the estimated OCV-SOC relations are consistent with the data from OCV tests at 0 °C, 25 °C, and 45 °C. With the above analysis, we can see that the proposed algorithm derives an accurate model describing battery behaviors.

4.2 SOC estimation

In this section, we evaluate the SOC estimation with the identified battery model obtained from the modeling experiment. The generality and robustness of SOC estimators are verified using FUDS and BJDST profile datasets. In initialization, we set $\boldsymbol{x}_0 = [10^{-6}, 10^{-6}, 0.8]^\top$ and $\sigma_x^2 = 10^{-3}$ [V^2].
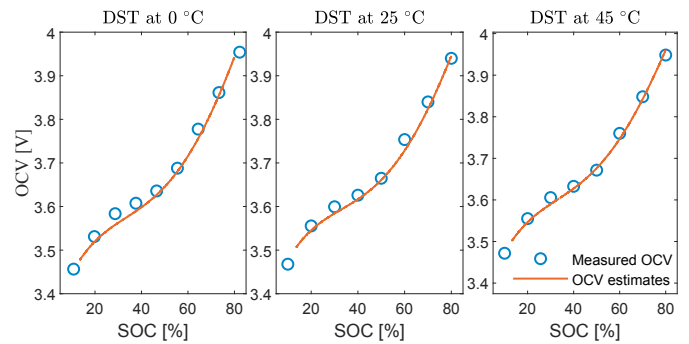

Fig. 4. Comparisons of OCV-SOC curves under DST at three different constant temperatures.

Fig. 5 shows the SOC estimates, reference SOC, and the estimation error on the FUDS and BJDST datasets at 0 °C, 25 °C and 45 °C. From the figure we can see that the estimated SOC aligns with the tested data in all six cases. Table 2 compares the root mean square SOC estimation error of the PF-RLS to the reference SOC with that of the online estimator (Zheng et al. (2016)) under FUDS and BJDST conditions at different temperatures. The best results are highlighted in bold. The proposed method presents lower RMSEs in most cases, outperforming the online estimator under different conditions and at different temperatures. Under FUDS and BJDST conditions, the SOC estimation errors of these approaches are larger at 0 °C, because the accuracy of the battery models at 0 °C is less than that at 25 °C and 45 °C, as shown in Table 1.
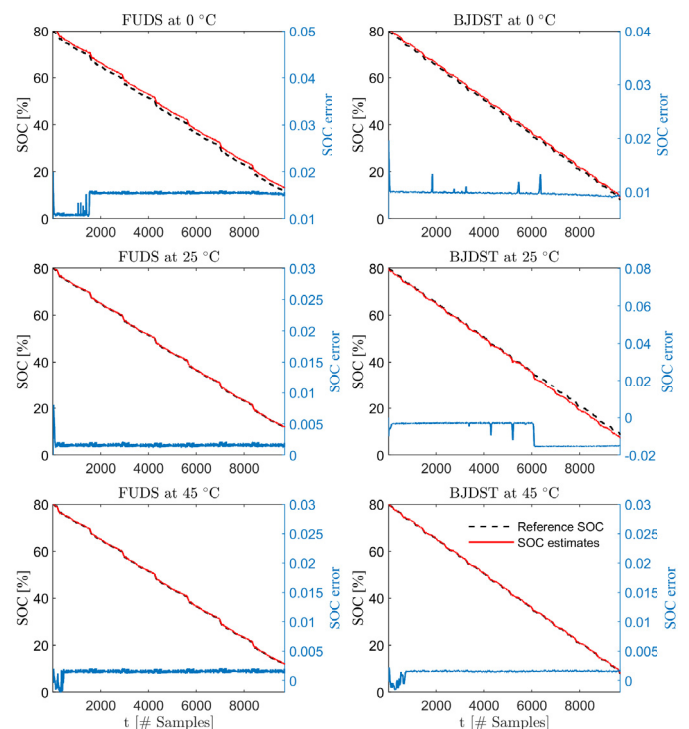

Fig. 5. SOC estimation results under FUDS and BJDST at three different constant temperatures.

The above-mentioned discussions are based on results obtained when applying the true initial SOC during estimation. To evaluate the convergence and the robustness of the SOC estimator for inaccurate initial values, we conduct the

Table 2. RMSE [mV] of SOC estimates at different operation conditions and temperatures.

Approaches	Conditions	0 °C	25 °C	45 °C
PF-RLS	FUDS	**14.90**	**1.60**	**1.50**
	BJDST	**9.80**	9.70	**1.50**
Online estimator	FUDS	39.00	3.50	8.30
	BJDST	42.00	**4.00**	5.00

SOC estimation with initial values that are $\pm10\%$ different from the true values. Table 3 presents the comparison of the RMSEs of the SOC estimation for the PF-RLS algorithm and the online estimator (Zheng et al. (2016)) with errors in the initial SOC of 0%, +10%, and −10% under FUDS test at 25 °C. Overall, the tracking result is satisfactory, and the PF-RLS shows smaller RMSEs than the online estimator in all three cases.

Table 3. RMSE [mV] of SOC estimates under FUDS with different initial SOC at 25 °C.

Approaches	Error of initial SOC guess		
	0%	+10%	−10%
PF-RLS	**1.60**	**4.80**	**3.60**
Online estimator	3.60	11.21	12.92

Fig. 6 shows the visual comparison of the SOC estimation of PF-RLS at different initial SOCs with the reference SOC computed by current integration (3). The left subplot shows these comparisons over the entire discharging cycle, and the right subplot shows that the proposed method quickly corrects the SOC values within two hundred iterations, and has good robustness and high estimation accuracy at different initial SOCs.
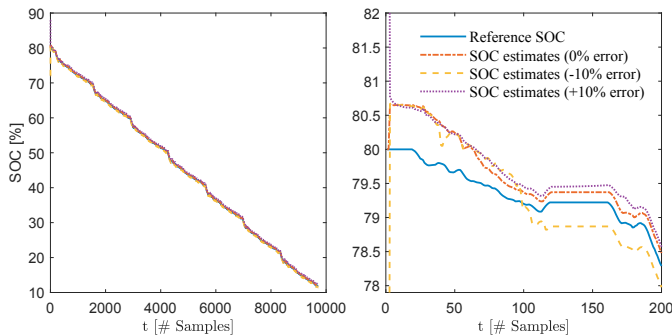

Fig. 6. SOC estimation results under FUDS at 25 °C with different initial guess errors. The right figure is a zoom in of the left figure for the first 200 samples.

5. CONCLUSION

This work develops a time-invariant grey box state-space model for Li-ion batteries considering the SOC dependency of the ECM model. The online concurrent state and parameter estimation is proposed to identify the grey box model by operating the recursive least squares parameter estimation and the particle filter with systematical resampling alternately. Finally, we verify the proposed model and algorithm on an NMC/Graphite Li-ion battery example demonstrating a superior performance over state-of-the-art approaches in aspects of the terminal voltage estimation accuracy and SOC estimation accuracy and robustness.

REFERENCES

Arulampalam, M.S., Maskell, S., Gordon, N., and Clapp, T. (2002). A tutorial on particle filters for online nonlinear/non-gaussian bayesian tracking. *IEEE Transactions on Signal Processing*, 50(2), 174–188.

Chen, M. and Rincon-Mora, G.A. (2006). Accurate electrical battery model capable of predicting runtime and iv performance. *IEEE transactions on energy conversion*, 21(2), 504–511.

Desai, T., Oliva, F., Ferrari, R.M., and Carnevale, D. (2023). Real-time battery state of charge and parameters estimation through multi-rate moving horizon estimator. *IFAC-PapersOnLine*, 56(2), 6124–6129.

Fan, K., Wan, Y., and Jiang, B. (2022). State-of-charge dependent equivalent circuit model identification for batteries using sparse gaussian process regression. *Journal of Process Control*, 112, 1–11.

Li, T., Bolic, M., and Djuric, P.M. (2015). Resampling methods for particle filtering. *IEEE Signal Processing Magazine*, 32(3), 70–86.

Meng, J., Luo, G., Ricco, M., Swierczynski, M., Stroe, D.I., and Teodorescu, R. (2018). Overview of lithium-ion battery modeling methods for state-of-charge estimation in electrical vehicles. *Applied sciences*, 8(5), 659.

Plett, G.L. (2004). Extended kalman filtering for battery management systems of lipb-based hev battery packs: Part 3. state and parameter estimation. *Journal of Power sources*, 134(2), 277–292.

Plett, G.L. (2015). *Battery management systems, Volume I: Battery modeling*, volume 1. Artech House.

Shrivastava, P., Soon, T.K., Idris, M.Y.I.B., and Mekhilef, S. (2019). Overview of model-based online state-of-charge estimation using kalman filter family for lithium-ion batteries. *Renewable and Sustainable Energy Reviews*, 113, 109233.

Tian, J., Liu, X., Li, S., Wei, Z., Zhang, X., Xiao, G., and Wang, P. (2023). Lithium-ion battery health estimation with real-world data for electric vehicles. *Energy*, 270, 126855.

Tian, N., Wang, Y., Chen, J., and Fang, H. (2020). One-shot parameter identification of the thevenin's model for batteries: Methods and validation. *Journal of Energy Storage*, 29, 101282.

Tran, M.K., Mathew, M., Janhunen, S., Panchal, S., Raahemifar, K., Fraser, R., and Fowler, M. (2021). A comprehensive equivalent circuit model for lithium-ion batteries, incorporating the effects of state of health, state of charge, and temperature on model parameters. *Journal of Energy Storage*, 43, 103252.

Wang, D., Yang, Y., and Gu, T. (2023). A hierarchical adaptive extended kalman filter algorithm for lithium-ion battery state of charge estimation. *Journal of Energy Storage*, 62, 106831.

Zhang, C., Allafi, W., Dinh, Q., Ascencio, P., and Marco, J. (2018). Online estimation of battery equivalent circuit model parameters and state of charge using decoupled least squares technique. *Energy*, 142, 678–688.

Zheng, F., Xing, Y., Jiang, J., Sun, B., Kim, J., and Pecht, M. (2016). Influence of different open circuit voltage tests on state of charge online estimation for lithium-ion batteries. *Applied energy*, 183, 513–525.